INSTITUT DE FRANCE
Académie des sciences

# Comptes Rendus

# Géoscience

## Sciences de la Planète

Nazanin Eslamirezaei, Seyed Ahmad Alavi, Seyed Tohid Nabavi
and Mohammad Reza Ghassemi

**Influence of multiple décollement and cover rock rheology on the structural evolution of thin-skinned fold-and-thrust belts: insights from discrete element modelling**

Volume 355 (2023), p. 215-236

Published online: 27 June 2023

https://doi.org/10.5802/crgeos.224



*Les* Comptes Rendus. Géoscience — Sciences de la Planète *sont membres du Centre Mersenne pour l'édition scientifique ouverte*
www.centre-mersenne.org
e-ISSN : 1778-7025

*Comptes Rendus*
*Géoscience — Sciences de la Planète*
**2023**, Vol. 355, p. 215-236
https://doi.org/10.5802/crgeos.224

Research article — Tectonics, tectonophysics, geodynamics

# Influence of multiple décollement and cover rock rheology on the structural evolution of thin-skinned fold-and-thrust belts: insights from discrete element modelling

**Nazanin Eslamirezaei** *, [a], **Seyed Ahmad Alavi** [a], **Seyed Tohid Nabavi** [a] and **Mohammad Reza Ghassemi** [b]

[a] Faculty of Earth Sciences, Department of Geology, Shahid Beheshti University, Tehran, Iran

[b] Research Institute for Earth Sciences, Geological Survey of Iran, Tehran, Iran

*E-mails:* nazanin.eslami@gmail.com (N. Eslamirezaei), a-alavi@sbu.ac.ir (S. A. Alavi), tohidnabavi@gmail.com (S. T. Nabavi), ghassemimr@gmail.com (M. R. Ghassemi)

**Abstract.** A variety of thin-skinned fold-and-thrust belts are associated with multiple décollements, which have low frictional basal and intermediate décollements related to mechanical stratigraphy and or overpressure conditions. The present study considers six ternary series of numerical discrete element (DE) models to simulate and explore the effects of mechanical stratigraphy with varied décollement layers, the number of cover sequences and thickness in the structural style, evolution, and strain partitioning of thin-skinned fold-and-thrust belts. Horizontal layer-parallel shortening of particles was induced by horizontal motion of a vertical boundary wall. The modelling results show weak décollements promoted the decoupled deformation of the fold-and-thrust belt with continues shortening. The results indicate that shortening was mainly accommodating by thrust-related folds with significant differences in the structural style. The formation of décollement, box, fault-propagation, and fault-bend folds, as well as extensional faults represents the ultimate style of the fold-and-thrust belts developed in DE-models. DE-models with thin and fewer number of décollements demonstrate that box-shaped décollement folds with less secondary disharmonic folds developed in the limbs of main fold structures. Furthermore, DE-models with thickest upper décollements are characterized by structural decoupling, more flow of material into the core of anticlinal structures and formation of complicated structures. The results of this study show that the structural style and decoupling can be affected by the rheology, number, and thickness of décollements. The DE-modelling results compared with natural examples, as well as analogue and numerical models, show that our mechanical modelling can overall match thin-skinned fold-and-thrust belts with multiple décollements that present different structural style.

**Keywords.** Structural style, Mechanical evolution, Multiple décollements, Thin-skinned tectonics, Fold-and-thrust belt, Discrete element model.

*Manuscript received 24 January 2023, revised 9 May 2023, accepted 8 June 2023.*

* Corresponding author.

## 1. Introduction

Field-based observations, seismic reflection profiles, balanced and restored crustal-scale sections, as well as analogue and numerical models demonstrated the geometry and kinematics observed in contractional settings such as fold-and-thrust belts are controlled by various factors. These factors have been studied, such as the presence of pre-existing structures [e.g., Nilforoushan et al., 2013, Nabavi et al., 2020, Del Ventisette et al., 2021, Najafi et al., 2021, Shamszadeh et al., 2022a], basement morphology and thrust ramp dip angle [e.g., Maillot and Koyi, 2006, Rosas et al., 2017, Caër et al., 2018, Ghosh et al., 2020], the depositional environment, mechanical stratigraphy (i.e. the mechanical properties, thickness of layers, and interface properties of rock units) [e.g., Cruz et al., 2008, Farzipour-Saein and Koyi, 2014, Pla et al., 2019, Ito and Moore, 2021], the presence of décollements (single and/or multiple) and their initial configurations [e.g., Sherkati et al., 2006, Stockmal et al., 2007, Graveleau et al., 2012, Nilforoushan et al., 2012, Ruh et al., 2012, 2013, 2017, Watkins et al., 2014, Ghanadian et al., 2017a,b, Li and Mitra, 2017, Borderie et al., 2018, Derikvand et al., 2018, 2019, Heydarzadeh et al., 2020, Gu et al., 2021, Eslamirezaei et al., 2022, Mohammadrezaei et al., 2022], the basal slope and velocity [e.g., Rosas et al., 2017], the basal friction [e.g., Cotton and Koyi, 2000, Costa and Vendeville, 2002, Koyi and Maillot, 2007], the angle of convergence [e.g., Casas et al., 2001, McClay et al., 2004, Leever et al., 2011, Barcos et al., 2016, Nabavi et al., 2017a,b, 2020], strain rate [e.g., Smit et al., 2003, Ruh et al., 2014], and syn-kinematic (syn-tectonic) surface processes (i.e. sedimentation and erosion) [e.g., Pichot and Nalpas, 2009, Cruz et al., 2010, 2019, Wu and McClay, 2011, Driehaus et al., 2014, Derikvand et al., 2019, Pla et al., 2019, Dal Zilio et al., 2020, Xu et al., 2021]. A class of fault-related folds is décollement folds, which are folding of more competent layers above a weak décollement without a ramp fault coring the uplift with a decreasing in displacement on a décollement [Mitra, 2003, Fossen, 2016, Nabavi and Fossen, 2021]. A variety of thin-skinned fold-and-thrust belts (i.e. décollement-dominated interpretive structural style and where deformation restricted to the sedimentary cover above the décollement level) are developed associated with multiple décollements such as the Zagros fold-and-thrust belts [e.g., Sepehr and Cosgrove, 2004, Sherkati et al., 2006, Vergés et al., 2011, Yosefnejad et al., 2017, Derikvand et al., 2018, Meng and Hodgetts, 2019a, Shamszadeh et al., 2022b], the Jura Mountains [e.g., Schori et al., 2015], the Pyrenees [e.g., Koyi and Sans, 2003], which exhibit low basal, intermediate and even upper friction related to lithology (salt, shale, marl) and/or overpressure conditions.

Many studies have already recognized that the density and thickness of décollements have played a significant role in the structural evolution and style, strain distribution and partitioning, controlling coupling and decoupling processes, and syn-kinematic processes in thin-skinned fold-and-thrust belts [e.g., Cotton and Koyi, 2000, Koyi et al., 2000, Mitra, 2003, Sherkati et al., 2005, Vergés et al., 2011, Ruh et al., 2012, 2013, Schori et al., 2015, Meng and Hodgetts, 2019a,b, Gu et al., 2021, Nabavi and Fossen, 2021, Sun et al., 2021, Xu et al., 2021]. Low-friction décollement is much weaker than any other layer in the rock sequences, so allowing material to flow at geologically high strain rates in response to normal and shear stresses of around 1 MPa. Moreover, portions dominated by folding are commonly underlain by a low-friction décollement and the flow of weak material into the cores of anticlinal structures may be inevitable for the evolution of décollement folds [e.g., Burberry et al., 2010, Cui et al., 2019].

Although previous studies have achieved an understanding of the role of décollements in the structural evolution of thin-skinned fold-and-thrust belts. This issue remains questionable, and numerical models provide an understanding of deformation patterns and structural styles. Proper interpretation of the structural evolution and structural style are essential to build the accurate understanding of the surface and subsurface geometry of structures. In this way, numerical modelling using discrete element method (DEM), as a particle-based method, provides means for simulating and tracking the spatial and temporal evolution of stress distribution, strain localization and sequential evolution of structures. It has been recognized that fold-and-thrust belts evolved in décollement-dominated way and exhibit wide range of structural styles, different fault-fold interactions, and associated fault-related folds, the mechanical conditions that contribute to these variations have not well to be understood.

This study makes use of a series of discrete element numerical models using the Itasca Particle Flow Code (PFC3D®, version 6,13, Itasca Consulting Group) to investigate the formation, development and evolution of thin-skinned fold-and-thrust belt comprising pre-kinematic low-frictional décollements , the number of décollements, thickness of décollements, the sequence of competent and less competent layers within the sedimentary cover sequence under an applied horizontal pressure and the amount of shortening. In this context, the present study aims to understand how the presence of low-friction multiple décollements influence the deformation style of thin-skinned fold-and-thrust belts. These mechanical properties have a direct influence on the deformation pattern of individual layers as well as the entire stratigraphic sequence.

Geological processes such as diagenesis, erosion, fluid flow, temperature, etc. are not considered. The primary reason for this approach is that we seek to isolate the effects of a few selected parameters in order to keep the analysis traceable. Besides, the numerical models can provide a powerful tool both to help interpret the structural style affected by décollements that may be poorly imaged on seismic profiles and previous models and to understand the kinematics and mechanics of fold-and-thrust belts which include more than a décollement. Finally, the modelling results of the present study are compared with natural examples, as well as analogue and numerical models.

## 2. The discrete element modelling method (DEM)

### 2.1. *Basic principles*

To develop an accurate understanding of the geometry of structures, the detailed analysis of structural evolution and structural style is needed. Numerical modelling using the Discrete Element Method (DEM) can simulate and monitor the spatial and temporal evolution of stress distribution as a particle-based approach. DEM, in except of time-consuming calibration of particle parameters to material properties, is an effective method to investigate the initiation, propagation, interaction and linkage, and evolution of folding, fracturing, and faulting in a practical manner involving deformation and large relative displacements.Many previous researches have used the DE-models and have been successfully produced realistic styles of geological and tectonic features such as normal faulting in layered sequences [e.g., Botter et al., 2014, Hardy, 2019], décollement folding [e.g., Hardy and Finch, 2005, Eslamirezaei et al., 2022], fault-bend folding [e.g., Benesh et al., 2007, Hughes et al., 2014], fault-propagation folding [e.g., Hardy and Finch, 2006, Hughes and Shaw, 2015], and fold-and-thrust belts [e.g., Burbidge and Braun, 2002, Hardy et al., 2009, Morgan, 2015, Meng and Hodgetts, 2019a,b].

A series of DE-mechanical models, are applied for simulation of deformation of the rock layers in a shortening setting. In this approach that uses a time stepping, finite difference approach to solve Newton's equations of motion, the rock mass is assumed to be composed of soft-circular, disk, or disc particles that interact in pairs as if bound by breakable elastic bonds (springs) and move relative to one another. These particles interact with elastic, gravitational, frictional and viscous forces under applied forces and displacement boundary (or wall) conditions. At each discrete time step, the particles are displaced to their new positions within the model by integrating their equations of motion using Newtonian laws and a velocity-Verlet-based numerical scheme, which is a numerical method used to integrate Newton's equations of motion as this integrator strike a good balance between computational cost, stability, and accuracy [Verlet, 1967]. The particle bonding is controlled by normal and shear bond stiffness, bond strength, and bond radius. In this regard, the normal and shear contact forces (Mohr–Coulomb criterion) are calculated between two overlapping or contacting particles using a rheological contact law. The bonds can be broken when the inter-particle forces exceed the bond strength. In this respect, slip can occur between particles. Thus, discontinuities and heterogeneities can form and evolve in response to changing stress condition and material properties [e.g., Cundall and Strack, 1979, Hardy et al., 2009, Hughes et al., 2014, Morgan, 2015, Smart et al., 2011, Hardy, 2019, Meng and Hodgetts, 2019a,b, Eslamirezaei et al., 2022].

### 2.2. *Model setup*

In the present study, we present a series of particle-based DE-models using the Itasca Particle Flow Code,

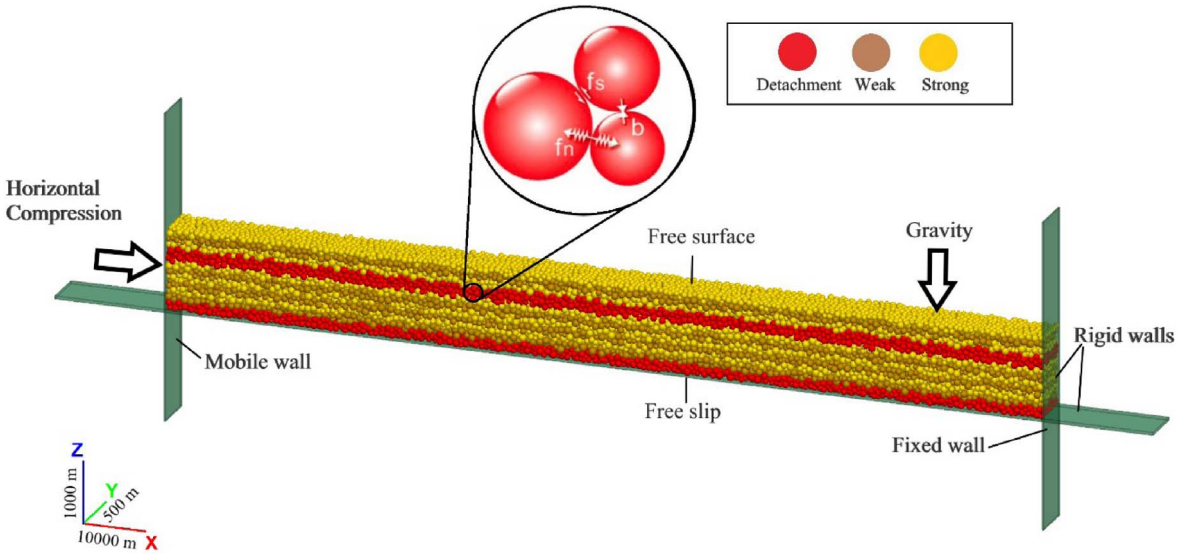


**Figure 1.** Initial design and boundary condition of discrete element models. Models are consisted of a basal décollement and adjacent layers of less competent and competent layers; middle and upper décollements will have added in the process of modelling. The $f_s$ = shear stress, $f_n$ = normal stress and $b$ is particle bond.

named PFC3D® software package (vers3ion 6.13, Itasca Consulting Group, https://www.itascacg.com/software/pfc). PFC® was initially developed for describing mechanical behavior of material (soil or rocks) and allows much flexibility in simulations and is widely used among geologists as it allows to model large deformations. We created a regular initial model (Figure 1) consisting of 21403 spherical particles in the part of upper crust model with dimensions of 10 km length × 1 km width × 0.5 km thickness ($x, y, z$). The particles radii range from 25 to 41 m for both décollements and cover layers following the Gaussian distribution of particle size. The mechanically layered cover sequence consists of relatively competent layer and relatively less competent layers. The average rock density for all particles is about 3000 kg/m$^3$. Particle stiffness (both shear and normal) were assigned with values of $1\times10^9$, $0.5\times10^9$, and $0.1\times10^9$ N/m, respectively, for competent, less competent, and weak décollements, (Table 1). Interparticle friction (μ) was assigned as 0.5 for cover layers, whereas 0 for décollements that are frictionless to ensure their low strength [e.g., Morgan, 2015, Meng and Hodgetts, 2019a]. All over, we examined different models based on changing variations included décollement number and thickness and the position and number of competent and less competent layers within the sedimentary cover. Colored layered within the cover sequence above and adjacent to décollements serve as strain markers during progressive deformation of the models and indicate contrast in material properties.

Our experimental setup consists of a horizontal surface and four vertical model boundaries. All of these surfaces are defined in the models by rigid, frictional boundary walls (i.e. free-slip boundary conditions). Numerically, free surface boundary conditions are applied on the top model face, thus permitting self-consistent evolution of topography [Nabavi et al., 2020]. Acceleration due to gravity (9.81 m/s$^2$) is imposed throughout the deformation as a body force. In all study models, a horizontal, vertical, compressional load was imposed along the left sidewall [i.e. displacement-based boundary conditions; Nabavi et al., 2018, 2020]. All results are shown here after 10%, 20%, and 30% shortening which are, respectively, equal to 1000 m, 2000 m and 3000 m displacement on décollements. The shear strength is $5\times10^6$ and $2.5\times10^6$ for competent and less competent layers respectively.

**Table 1.** Summary of material properties and parameters used in 3D DE-models

| Parameters | Décollements layers | Overburden | |
|---|---|---|---|
| | | Less competent layers | Competent layers |
| Particle radius (m) | | 25–41 m | |
| Particle Stiffness (N/m) | $0.1 \times 10^9$ | $0.5 \times 10^9$ | $1 \times 10^9$ |
| Contact friction ($\mu$) | 0 | 0.5 | |
| Tensile bond strength (N) | 0 | $2.5 \times 10^6$ | $5 \times 10^6$ |
| Average density (kg/m$^3$) | | 3000 kg/m$^3$ | |

## 3. Modelling results

We present here the main features observed in the six series of DE-models after 30% (~3000 m displacement) orthogonal shortening to investigate the deformation and structural evolution of thin-skinned fold-and-thrust belts with multiple décollements (summarized in Table 2). Clearly, there are large number of décollements model setups that we could present, however, we discussed here: (1) the role of multiple décollements, (2) décollement thickness, (3) the number and mechanical properties of competent and less competent layers within the sedimentary cover, and (4) strain localization in the evolution of thin-skinned fold-and-thrust belts and their structural style using six series of DE-models which are based on progressive deformation events. In all models, the sedimentary cover sequence overly a décollement at the base of models. Furthermore, we consider more units as décollements to simulate multiple décollements models. Development and the evolution of deformation in a series of DE-models illustrate that displacement field vary in different parts of the fold and also a fold-and-thrust belts and they play an important role in fold geometries and the structural style of a contractional tectonic setting.

### 3.1. *Models with two décollements*

#### 3.1.1. *Series 1—an upper décollement surrounded by competent layers*

Model 1 (Figure 2) presents the effects of basal décollement and a thick intermediate décollement on the structural style and evolution of the sedimentary cover sequence consisted of a series of competent bonded layers (four competent layers thick) intercalated with less competent bonded layers (three less competent layers thick). Overall, after an initial step of homogeneous shortening of the model, the deformation is essentially pure-shear thickening (contraction or buckling) with the hinterland-verging low-amplitude asymmetric décollement fold at the onset of deformation. In this model, the first contractional structures such as asymmetric décollement folds and some fore-thrusts appeared after 20% bulk shortening. Also, completely detached rootless folds appeared above the intermediate décollement (Model 1c in Figure 2). After 30% of bulk shortening, the model shows disharmonic geometry of deformation within the layers due to the difference in propagation between the layers above and beneath the décollements from surface to deeper parts. Shortening led to development of more penetrative contractional structures such as back-thrusts, faulted décollement fold, and hinterland-verging fault-propagation fold (Model 1d in Figure 2). Also, some detached rootless folds above the intermediate décollement were still visible. Moreover, increasing shortening causes both flexural slip and flexural flow, respectively, in major shear zones and in the lower parts of fault-related folds so that they are filled with less competent material that evacuated beneath synclines and flowed into the anticline core.

Model 2 (Figure 2) is dominated by faulting, however, the dip angle of faults varies as shortening progresses and also in accordance with mechanical stratigraphy (composition). In this regard, the low angle or sole thrust fault was developed in the lower décollement and propagate upward within the overlying competent sediments so that faults passing through competent units are steeper than those within incompetent units (i.e. a faulted décollement fold structure). Hence, as deformation continued, the fault progressively elongated along basal and upper décollements and such variations in mechanical stratigraphy of the deformation setting leads to

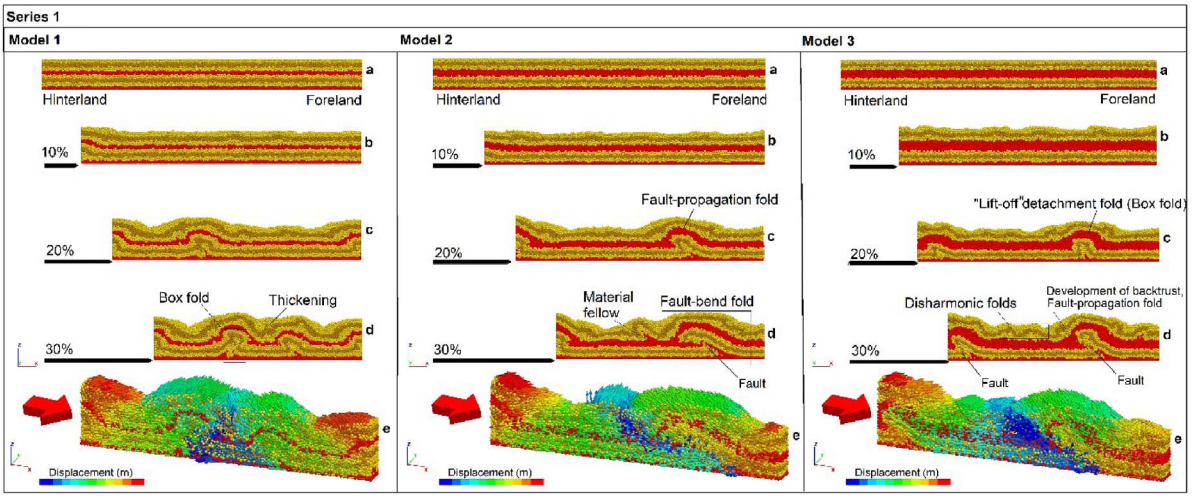


**Figure 2.** The velocity vectors for sedimentary sequence and the evolution of DEM to show the folding in the models 1, 2, and 3 of series 1 for sedimentary sequence with two décollements after 30% (3000 m displacement) orthogonal shortening in three steps of shortening 10%, 20%, and 30%. The models are the same in terms of the thickness of the basal décollement and different in the upper décollement with increasing thickness surrounded by competent layers.

**Table 2.** Summary of results of the discrete element models

| Model name | Series 1 | | | Series 2 | | | Series 3 | | | Series 4 | | | Series 5 | | | Series 6 | | |
|---|---|---|---|---|---|---|---|---|---|---|---|---|---|---|---|---|---|---|
| | 1 | 2 | 3 | 1 | 2 | 3 | 1 | 2 | 3 | 1 | 2 | 3 | 1 | 2 | 3 | 1 | 2 | 3 |
| Number of décollements | 2 | 2 | 2 | 2 | 2 | 2 | 2 | 2 | 2 | 3 | 3 | 3 | 3 | 3 | 3 | 3 | 3 | 3 |
| Main fold styles | BF | FPF FBF | BF FPF | FBF | FBF | FBF | BF | BF | BF | BF | BF | DF | BF | BF | BF DF | BF | FPF | DF BF |
| Décollement thickest | - | - | Intermediate | - | - | Intermediate | - | - | Upper | - | - | Intermediate Upper | - | - | Upper | - | - | Intermediate |

BF = Box Fold. FBF = Fold Bend Fold. FPF = Fold Propagation Fold. DF = Décollement fold.

the development of ramp–flat geometries and associated structures such as fault-bend folds, so that only one fault broke to the lower unit and thrust it up over the upper unit. Moreover, as deformation continued, the fault as a back-thrust progressively elongated until a second fault formed in front and propagated from the upper décollement to the surface, and also from the foreland to the hinterland. Shortening led to formation and development of more penetrative contractional structures such as backthrusts, faulted décollement fold. Also, some detached rootless folds and blind thrusts above the intermediate décollement were still visible. Total (relative) displacement magnitude and direction between the driving hinterland wall and the foreland wall are illustrated and colored as the characteristic of the tectonic shortening accommodated by internal deformation of the model (Model 2e in Figure 2). The primary control on throw partitioning in the model is fault displacement. The displacement magnitude field is smooth, fan-like and radiates from the basement fault tip. At low differential displacements, undeformed state to gentle folding of beds is the main contributor to deformation accommodated across

the contractional zone. Backthrusts occur also in the model and show relatively low displacement, so that slip is predominantly along forethrusts.

Model 3 (Figure 2) shows a simulation of sedimentary layers with intermediate décollement, which affect the structural style and evolution of the sedimentary cover sequence consisted of a series of competent bonded layers (four competent layers thick) intercalated with less competent bonded layers (two less competent layers thick). After 20% bulk shortening, the lower structural level of the study model initially forms a lift-off detachment fold, and subsequently became a hinterland-verging asymmetric décollement anticlinal structures as a backthrust to accommodate the deformation. The upper level shows a train of buckle folds without any geometric connection to the lower part. After 30% bulk shortening, asymmetric décollement folds in the lower structural level of the study model evolve into hinterland-verging fault-propagation folds cored by the basal décollement material (i.e. a faulted décollement fold structure). Furthermore, shortening was accommodated by the formation of new buckle folds and also amplification and tightening of existing folds in the upper level (Model 3d in Figure 2). Underlying folds vergence in the same direction as the overlying structures, suggesting that deformation has been only partially decoupled across the intermediate décollement.

#### 3.1.2. *Series 2—an upper décollement surrounded by less-competent layers*

In Series 2 (Figure 3) we investigate the effect of basal and upper décollements and the upper décollement variation in thickness on structural style and evolution of sedimentary cover sequences consisted of a series of less competent bonded layers (four less competent layers thick) intercalated with competent bonded layers (two competent layers thick). Overall, after an initial step of homogeneous shortening of model 1 of series 2 experiments, deformation initiates by pure-shear thickening that caused formation of two low-amplitude asymmetric folds with disharmonic minor folds and thickening in both limbs near hinterland and un-deformation in foreland at the onset of deformation. In this model, the first contractional structures such as low amplitude asymmetric folds and some disharmonic folds appeared after 20% of shortening (Model 1c in Figure 3). Furthermore, the folding accompanied by uplift and martial flow toward the core of anticlines and formation of extensional fracture/faults in the intermediate décollement or forelimb of main fold in final step after 30% of shortening. At the end of experiment, the model shows a general fault-bend style of folding, in which shortening led to formation of detached rootless folds above décollement layers (Model 1d in Figure 3). In model 2 with thicker décollement, the early stage of shortening and deformation started by formation of foreland-verging fault-propagation fold which was developed in the further stage by pure shear fault bend fold and the height of the model increased as a result of contraction in the 20% of shortening (Model 2c in Figure 3). As bulk shortening continues, fault segments were penetrated in the layers beneath the upper décollement and propagated upward by shortening (Model 2c in Figure 3). In the 30% of shortening the thickening of upper décollement appeared and deformation developed by formation of asymmetric low amplitude fold with structural decupling in final stage in 30% (Model 2d in Figure 3).

In model 3 that was run to show a simulation of sedimentary layers consisted of a series of less competent bonded layers (four less competent layers thick) interacted with competent bonded layers (two competent layers thick) with thickest intermediate décollement in this series (Figure 3). Deformation initiates by formation of two main low amplitude folds in 20% of shortening (Model 3c in Figure 3) that developed to fault bend style in 30% of shortening (Model 3d in Figure 3). The thickening in the upper décollement was visible and structural decupling occurred by formation of asymmetric folds in surficial layers. Furthermore, disharmonic folds formed as a result of shortening at the final stage. The shortening was accommodated by uplift and folding. Total (relative) displacement magnitude and direction between the driving hinterland wall and the foreland wall are illustrated and colored for all models (Models 1e, 2e and 3e in Figure 3).

#### 3.1.3. *Series 3—basal and upper décollements separated by sedimentary layers*

In the series 3 (Figure 4) we investigated the effects of basal and upper décollements and the variation in thickness of upper one on the structural style and evolution of the sedimentary cover sequence

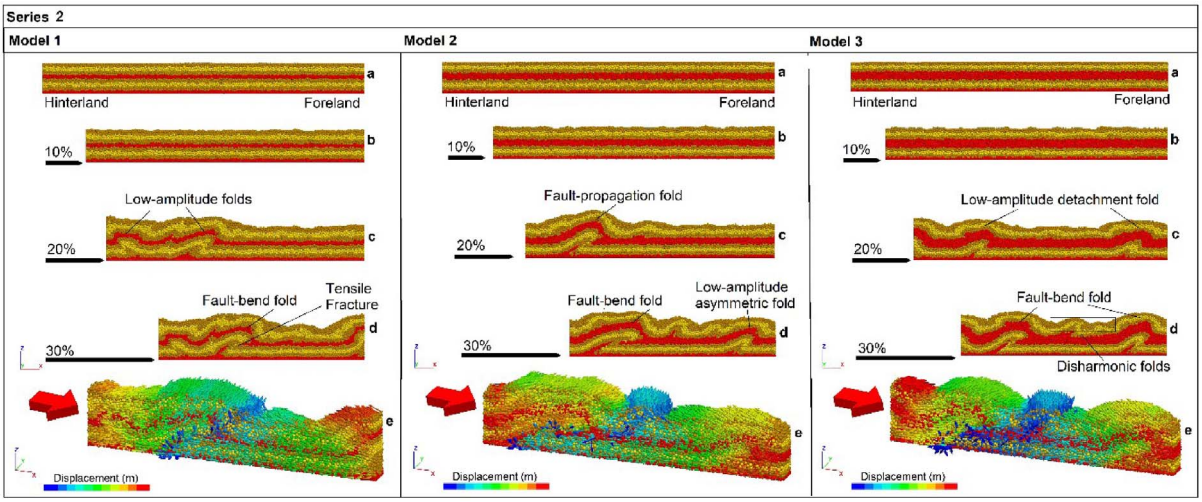


**Figure 3.** The velocity vectors for sedimentary sequence and the evolution of DEM to show the folding in the models 1, 2, and 3 of series 2 for sedimentary sequence with two décollements after 30% (3000 m displacement) orthogonal shortening in three steps of shortening 10%, 20%, and 30%. The models are the same in terms of the thickness of the basal décollement and different in the upper décollement with increasing thickness surrounded by less competent layers.

consisted of multiple competent and less competent bonded layers that separated basal and upper décollements. In model 1 of series 3 experiments the thickness of décollements is equal to other sedimentary layers. In the first stage of homogeneous shortening, deformation initiates by flexural slip next to the hinterland that produced disharmonic folds. Moreover, in the center of the model a compressional box-shaped décollement fold structure with two axial surface and disharmonic folds in its limbs formed (Model 1c in Figure 4). This box fold become tighten and developed by uplift until 30% of shortening (Model 1d in Figure 4).

In model 2 of series 3 experiments the upper décollement is thicker so deformation started by formation of symmetric décollement folds. In the 20% of the shortening deformation continued by distortion in the layers beneath the upper décollement and thickening in the décollement layer (Model 2c in Figure 4). The layers located on upper décollement showed the low steep folding. Such fold structures subsequently became a hinterland-verging fault-propagation folds caused by the thickness and rheology of the upper décollement to accommodate the deformation (Model 2c in Figure 4). The model 3 of series 3 experiments represents the effect thickest upper décollement on the structural style of sedimentary sequence. In the 20% of shortening, the asymmetric box-shaped folds appeared that developed along with formation of minor disharmonic folds (Model 3c in Figure 4). The shortening accommodated by formation of disharmonic folds in the layers above the upper décollement. Shortening led to development of contractional structures such as faulted décollement fault, lift-off and box-shaped folds above and beneath the upper décollement (Model 3d in Figure 4). Total displacement magnitude and direction between the driving hinterland wall and the foreland wall are illustrated and colored for all models as the characteristic of the tectonic shortening accommodated by internal deformation of the model (Models 1e, 2e and 3e in Figure 4).

## 3.2. *Models with three décollements*

### 3.2.1. *Series 4—increasing thickness in intermediate and upper décollements*

The Series 4 (Figure 5) presents the effect of multiple décollements on the structural style and evolution of the sedimentary cover sequence consisted of a series of competent bonded layers (six competent layers thick) intercalated with weak, less

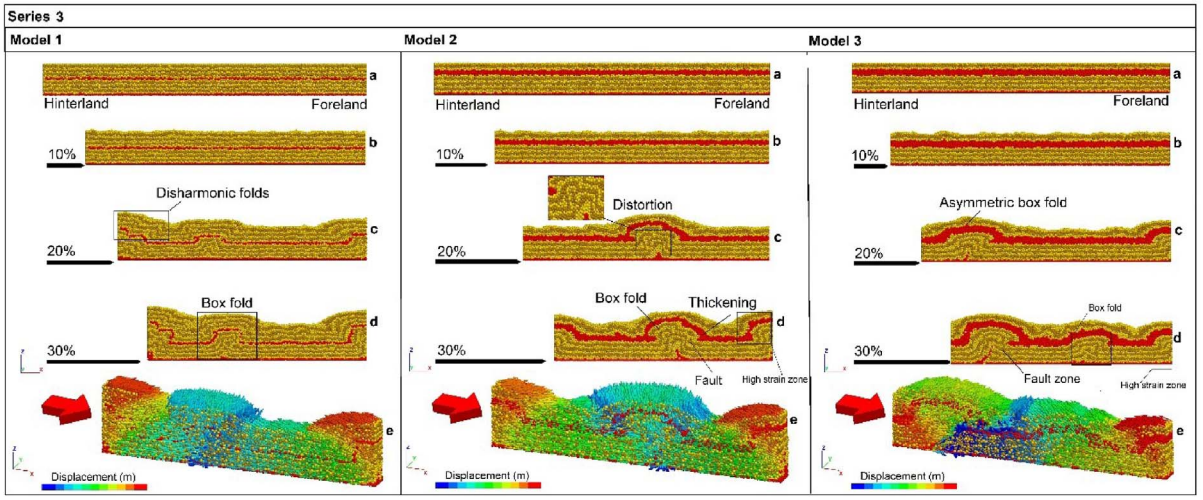


**Figure 4.** The velocity vectors for sedimentary sequence and the evolution of DEM to show the folding in the models 1, 2, and 3 of series 3 for sedimentary sequence with two décollements after 30% (3000 m displacement) orthogonal shortening in three steps of shortening 10%, 20%, and 30%. The models are the same in terms of the thickness of the basal décollement and different in the upper décollement with increasing thickness. Basal and upper décollements separated by several sedimentary layers.

competent bonded layers (three less competent layers thick). In this series of models, the thickness of intermediate and upper décollements increased simultaneously. At the onset of deformation applied on model 1 of series 4 experiments, shortening was accommodated by development of a series of box-shaped buckles in 20% of shortening (Model 1c in Figure 5) and the other box fold appeared in next step along with uplift in 30% of shortening and extensional fracture/faults appeared in the final stage (Model 1d in Figure 5). In model 2 of this series, the thickness of intermediate and upper décollement increased and deformation started by formation of small wavelength asymmetric lift-off décollement fold with disharmonic minor folds and fractures in less competent layers that developed further into box-shaped asymmetric fold (Model 2c in Figure 5). Such fold structures subsequently became a hinterland-verging fault-propagation folds caused by the thickness and rheology of intermediate and upper décollements to accommodate the deformation (Model 2c in Figure 5). In the next step of deformation, the layers are more tightened and other contractional structures formed as presented in 30% of bulk shortening (Model 2d in Figure 5).

The deformation in the Model 3 of Series 4 experiments started by formation of symmetric décollement fold that developed during shortening by uplift and also extensional fracture/faults in the upper décollement. Martial fellow from décollements into the core of anticline is visible at the 30% of shortening (Model 3d in Figure 5). The type of décollement folds in the final stage is chevron lift-off fold whereby the layers are isoclinally folded in the core of anticline and the ductile materials are flow from the core of the folds. The shortening was accommodated by decoupling, folding and uplift. Total displacement magnitude and direction between the driving hinterland wall and the foreland wall are illustrated and colored for all models (Models 1e, 2e and 3e in Figure 5) as the characteristic of the tectonic shortening accommodated by internal deformation of the model.

### 3.2.2. *Series 5—increasing thickness in the upper décollement*

Series 5 (Figure 6) presents to simulate the effects of three décollements on the structural style and evolution of the sedimentary cover sequence consisted of a series of competent bonded layers with the increasing thickness in the upper décollement. Overall, after an initial step of homogeneous shortening, the deformation initiates by flexural slip in the model 1 of series 5 experiments that caused the formation of symmetric box-shaped folds and disharmonic folds

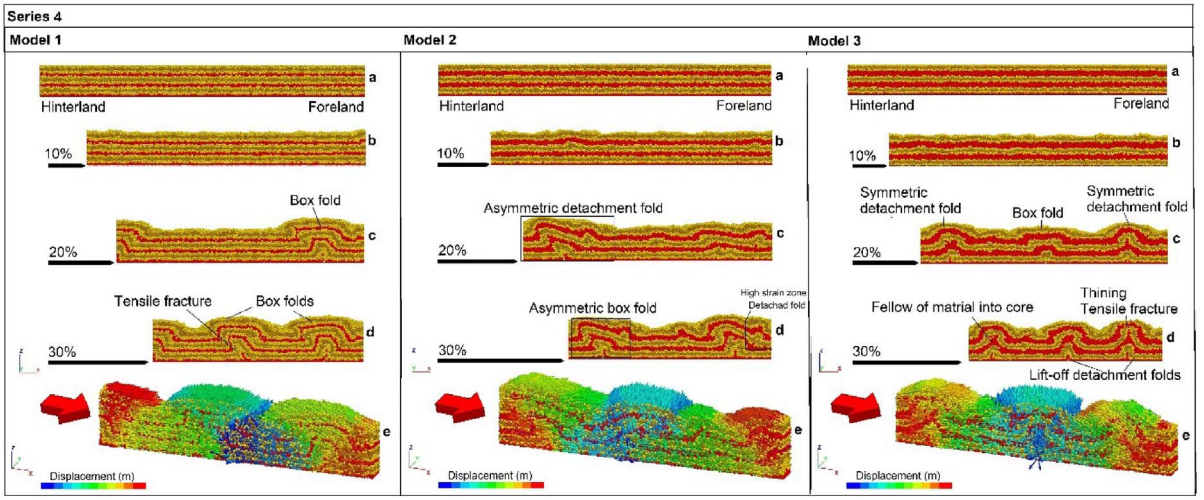


**Figure 5.** The velocity vectors for sedimentary sequence and the evolution of DEM to show the folding in the models 1, 2, and 3 of series 4 for sedimentary sequence with three décollements after 30% (3000 m displacement) orthogonal shortening in three steps of shortening 10%, 20%, and 30%. The models are the same in terms of the thickness of the basal décollement, intermediate and upper décollement with increasing thickness from 1 to 3.

in the 20% of shortening (Model 1c in Figure 6) that evolved in the further stages of deformation by uplift and also thickening in the sedimentary layers located in the limbs of folds after 30% of bulk shortening (Model 1d in Figure 6). In model 2 of series 5 of experiments with thicker upper décollement, the deformation initiates by formation of asymmetric folds in 20% of shortening (Model 2c in Figure 6). The folds progressively tighten and developed into lift-off to box fold. This main lift-off fold amplified toward the surface. The formation of forethrust in the core of box fold accrued in 30% of shortening and extensional fracture/faults in the intermediate décollement presents the strain localization (Model 2d in Figure 6). The shortening was accommodated by fold amplification.

In model 3 of series 5 experiments with thickest upper décollement the deformation started by formation of low amplitude fold and an asymmetric décollement fold without any faults or fractures in 20% of shortening (Model 3d in Figure 6). By increasing the shortening at the further steps in the 30% of shortening, the highly strain fold such as lift-off fold formed that contains the fractures in the core of anticline (Model 3d in Figure 6). These fractures in the layers beneath the upper décollement are the results of contractional environment and fold tightening. There are other disharmonic folds in the layers near the surface that are effective in the topography. Total (relative) displacement magnitude and direction between the driving hinterland wall and the foreland wall are illustrated and colored for all models (Models 1e, 2e and 3e in Figure 6) as the characteristic of the tectonic shortening accommodated by internal deformation of the model.

### 3.2.3. *Series 6—increasing thickness in the intermediate décollement*

In model series 6 (Figure 7) that represents the effect of multiple décollements and the variation in thickness of intermediate décollement on the structural style and evolution of the sedimentary cover sequence consisted of a series of competent bonded layers (six competent layers thick) intercalated with less competent bonded layers (three less competent layers thick).

In model 1 of series 6 experiments, deformation initiates by uplift and formation of single symmetric box-shaped décollement folds and also the disharmonic folds in sedimentary layers at the onset of deformation (Model 1c in Figure 7). By increasing shortening, the other box-shaped fold

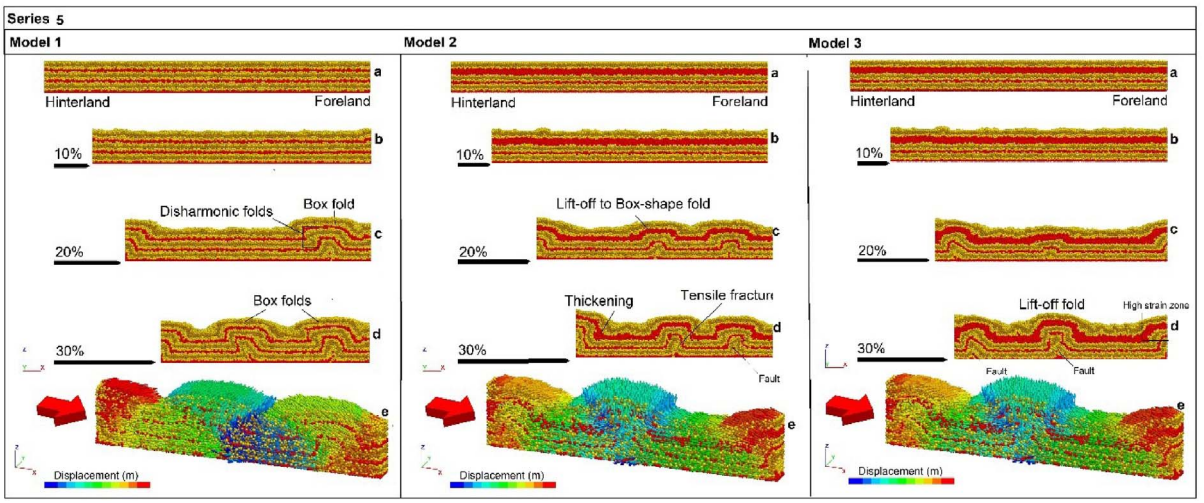


**Figure 6.** The velocity vectors for sedimentary sequence and the evolution of DEM to show the folding in the models 1, 2, and 3 of series 5 for sedimentary sequence with three décollements after 30% (3000 m displacement) orthogonal shortening in three steps of shortening 10%, 20%, and 30%. The models are the same in terms of the thickness of basal and intermediate décollements. The thickness of the upper décollement increases in the study models.

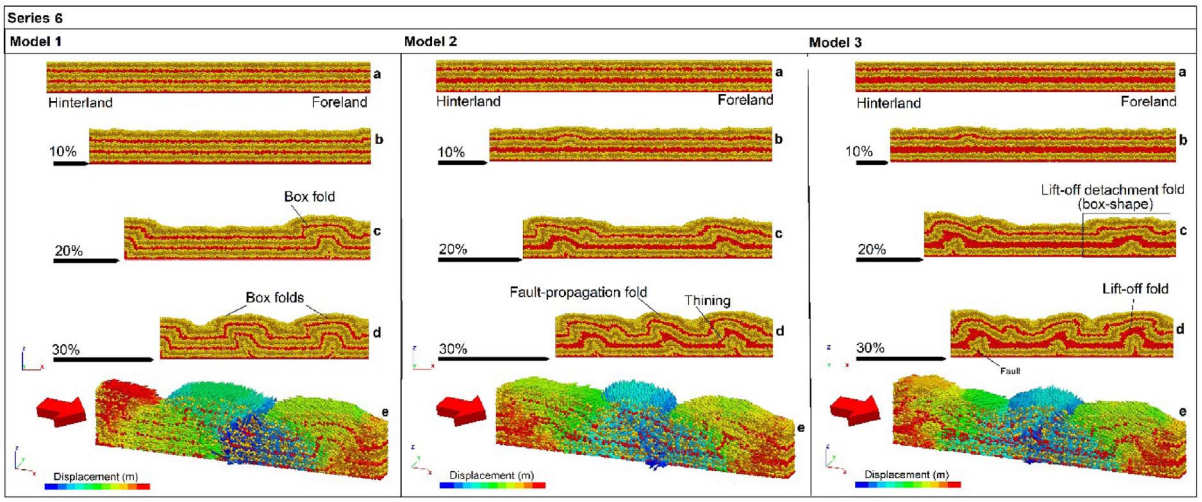


**Figure 7.** The velocity vectors for sedimentary sequence and the evolution of DEM to show the folding in the models 1, 2, and 3 of series 6 for sedimentary sequence with three décollements after 30% (3000 m displacement) orthogonal shortening in three steps of shortening 10%, 20%, and 30%. The models are the same in terms of the thickness of basal and upper décollements. The thickness of the intermediate décollement increases in the study models.

formed after 30% of bulk shortening (Model 1d in Figure 7). In model 2, minor fold structures developed subsequently became a hinterland-verging fault-propagation folds after 20% shortening due to the thickness and rheology of intermediate décollement to accommodate the deformation (Model 2c in

Figure 7). After 30% shortening, layers are isoclinally folded in the core of the anticline and the fold developed by uplift and formation of minor folds in the limbs of main folds and structural decoupling and thickening (Model 2d in Figure 7).

In model 3 of series 6 experiments with thickest intermediate décollement the deformation started by formation of rootless minor fold. As deformation continued in the next step of shortening, the low-amplitude lift-off décollement fold with extensional fracture/faults in the core of anticline appeared in the 20% of bulk shortening that evolved by uplift and formation of disharmonic minor folds (Model 3c in Figure 7). This fold is isoclinally folded in the core of the fold that named box lift-off (Model 3c in Figure 7). During progressive deformation, shortening was accommodated by uplift, decoupling, folding with an increase in limb dips at the final stage of the experiment. In this stage all minor and major folds are tightened and the chevron shaped lift-off fold formed (Model 3d in Figure 7). Total displacement magnitude and direction between the driving hinterland wall and the foreland wall are illustrated and colored for all models (Models 1e, 2e and 3e in Figure 7) as the characteristic of the tectonic shortening accommodated by internal deformation.

## 4. Comparison with a natural example: the Zagros fold-and-thrust belt of Iran

Décollements are necessary to form thin-skinned fold-and-thrust belts and their role has been studied for a long time [e.g., Wilkerson et al., 2007, Lacombe et al., 2016, Humair et al., 2020]. The DE-model results obtained in this study demonstrate that the presence, thickness, mechanical properties, and the number of décollements play key roles in controlling how contractional settings evolve. In this regard, styles of natural fold-and-thrust belts are compared to our modelling results to illustrate the geometry and kinematics of their evolution.

The Zagros orogenic belt, SW Iran, resulted from convergence and shortening between the Arabian plate and the Iranian continental block [Alavi, 2004, 2007, Mouthereau et al., 2012]. The Zagros orogenic belt can be divided into several structural zones along strike from the east to the west including the Fars, Izeh, Dezful Embayment, and Lurestan, based on their differences in structural style and tectono-sedimentary [e.g., Alavi, 2004, 2007, Mouthereau et al., 2012]. The Zagros fold-and-thrust belt is characterized by a broad symmetric to asymmetric, and gently to isoclinal fold geometries [Sherkati et al., 2005, 2006, Derikvand et al., 2018, Nabavi and Fossen, 2021, Shamszadeh et al., 2022b]. The dominant wavelength of such fold structures is $15.8 \pm 5.3$ km [Mouthereau et al., 2006]. The Zagros fold-and-thrust belt contains several evaporate and/or weak shale layers in the sedimentary sequence which are thick enough to form independent décollements. The nature and influence of the presence of multiple décollements are identified by many researches as an important controlling factor of the structural style in the Zagros belt [e.g., Sherkati et al., 2005, 2006, Sepehr and Cosgrove, 2004, Vergés et al., 2011, Farzipour-Saein and Koyi, 2014, Ghanadian et al., 2017a,b, Derikvand et al., 2018, 2019, Heydarzadeh et al., 2020, 2021, Koyi and Mansurbeg, 2021]. The Dezful Embayment in the Zagros foreland is a classic example of this case, where containing the world's largest hydrocarbon reserves in a fold belt. In the fold belt, as many as four Jurassic–Cretaceous shale units provide intermediate décollements above the deep Infracambrian Hormoz salt décollement.

Salt/shale-cored décollements folds and some isoclinal lift-off fold geometries are similar to those commonly reported from the other thin-skinned fold-and-thrust belts, however, thrust-related folds and the emplacement of thrust sheets have taken place here due to the presence of multiple décollement horizons [Pla et al., 2019]. Evaporite-cored anticlinal structures formed as décollement folds during tectonic shortening and the ductile flow of evaporite in the anticline core are resulting in an evaporite thickening. Subsequently, deformation is localized in the evaporite-cored anticlinal structure, which are structurally accommodated by fore-thrusts and back-thrusts generating fault-propagation folds and pop-up structures. Fishtail structures, which are a type of triangle zones in thrust systems, are also one of the other common structures in contractional deformation zones with multiple décollements. In this area, short wavelength anticlines in the Oligo-Miocene Asmari Formation are interpreted to be detached in the Pabdeh and Gurpi or in the Kazhdumi formations [Sherkati et al., 2005, Derikvand et al., 2018, 2019, Heydarzadeh et al., 2021, Shamszadeh et al., 2022b]. Above these shale décollements, the

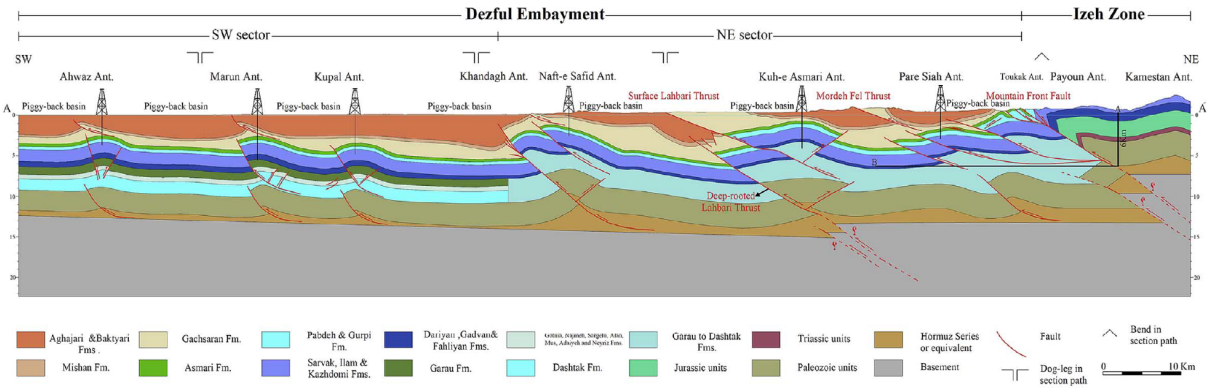


**Figure 8.** Structural cross-section on the southern part of the Izeh zone and the northern part of the Dezful Embayment. The Hormoz series and the Garau to Dashtak formations controlled the geometry of folds as the major décollement horizons [Derikvand et al., 2018].

Miocene Gachsaran Formation provides a shallow salt décollement 1 to 2 km thick in the Dezful Embayment [Sherkati et al., 2006, Ghanadian et al., 2017a,b, Derikvand et al., 2018, 2019]. Structural coupling across this shallow décollement is high, so that anticlines above the décollement tend to overlie anticlines below the décollement. In contrast, where structural coupling is low, folds form disharmonic geometries above and below the Gachsaran décollement, and create exploration challenges in the Asmari Limestone reservoir.

Furthermore, the Gachsaran evaporates may migrate from anticlines to adjacent synclines in the Lurestan structural zone, in which thrusts affecting the overlying sequences and develop significant disharmonic fold geometries. Such disharmonic fold geometries in the overlying Asmari Formation occurs where the thickness of the interposed incompetent units exceeds a critical thickness that leaves the Asmari limestone outside of the contact strain zone of the Bangestan limestones buckles. Disharmonic fold geometries, however, vanishes toward the southwest, where the Asmari limestone and the top of the Late Cretaceous Bangestan limestones are roughly concordant, implying a change in the décollement properties. Sedimentary package of the Oligocene–Miocene Shahbazan–Asmari unit and the Bangestan Group was folded harmonically and display short-wavelength in geometry [Casciello et al., 2009, Vergés et al., 2011, Farzipour-Saein, 2017]. Disharmonic décollement folds can be seen in DE-models of series 4 and also DE-models 2 and 3 of series 6 experiments in the present study that are buckle folds on different wavelength. Disharmonic fold geometries across décollements may produce sharp transition of geometric characteristics due to the interlayering of competent and incompetent beds. In addition, it should be noted that several parallel or concentric folding structures have been developed in Zagros fold-and-thrust belt. Such parallel folds exhibit broad anticlines and narrow synclines in the upper units and vice versa in the intermediate and upper décollements, that is particularly comparable with DE-models of series 4 experiments in the present study (i.e. Model 3c and 3d in Figure 5). Furthermore, the lithostratigraphic units between two major décollements in the Zeloi anticline (Dezful Embayment, SW Iran) display different fold geometries (Figure 8) [Derikvand et al., 2019], which is comparable with the model 3 of series 6 that has thicker intermediate décollement compared to the other two models. Overall, models with thick décollements show a further developed deformation and more complex fold and fault structures, partically in the overlying strata, at the final stage of shortening (i.e. 30%) compared to models with thin décollements (like the model 2 of series 6).

## 5. Comparison to previous modelling studies

Critical tapered-wedge theory has been successfully applied to the study of the deformation mechanism and kinematic evolution of fold-and-thrust belts and accretionary prisms in contractional settings

[e.g., Davis et al., 1983, Dahlen, 1984, 2003, Buiter, 2012]. The theory indicates that the critically tapered wedge, as a stable geometry, slides along the basal décollement without internal deformation and is dependent on the basal friction coefficient and the internal strength of the material. According to the modelling results, when the wedges are in subcritical or supercritical states, the ramp–flat structure and vertical uplift in the hinterland increases the slope angle to approach the critical angle. Furthermore, hinterland-verging fault-propagation folds, as a backthrust, were developed in DE-models when the wedge at the front of the deformation belt is in a subcritical state, backthrusting along the intermediate and/or upper décollement steepens the wedge so as to approach the critical angle.

Many thin-skinned fold-and-thrust belts are formed above multiple décollements producing different structural styles with complicated fold and fault geometries. So that, fold geometry in fold-and-thrust belts is an important issue for hydrocarbon exploration [Nabavi and Fossen, 2021]. In thin-skinned fold-and-thrust belts, décollements are frequent, and their impact has long been explored by means of various techniques [Davis and Engelder, 1985, Homza and Wallace, 1995, Konstantinovskaya and Malavieille, 2011, Gu et al., 2021]. In this regard, the structural evolution of thin-skinned fold-and-thrust belts has been investigated in several analogue and numerical models. Overall, there is a general agreement between our numerical modelling results with scaled analogue and numerical models that simulating the evolution of multiple décollement thin-skinned fold-and-thrust belts.

Ghanadian et al. [2017b] (Figure 9) have documented how an additional intermediate décollement and its thickness variations promotes folding and thrusting of the heterogeneous sedimentary sequence in the Dezful Embayment, as well as the role of strain rate. We numerically obtained a similar evolution with two décollements that the upper décollement surrounded by competent layers (i.e. series 1 experiments in this study) and three décollements in which the intermediate décollement thickness varies (i.e. series 6 experiments in this study) (Figure 7). Farzipour-Saein [2017] and Farzipour-Saein and Koyi [2014] also investigated the structural effects of basal and intermediate décollements in the Lurestan, Fars and Izeh structural zones using a series of scaled sand-box analogue models. Their results and our numerical models with two weak décollements are comparable.

Furthermore, the analogue modelling results by Pla et al. [2019] demonstrate that as the viscosity of the décollement increases, the deformation propagates more slowly from hinterland to the foreland part of the fold-and-thrust belt, and the underlying thrust stack becomes broader and lower and has a gentler thrust taper angle. The rheology of the décollement defines the distribution and geometry of the sedimentary cover detached on it that in turn influence the structural style and development of fold and thrust structures.

Moreover, Cui et al. [2020] investigated the role of a strong basal décollement and a weak upper décollement with different strengths by a series of analogue models to simulate the structural style and deformation patterns of the Longmen Shan fold-and-thrust belt, eastern margin of the Tibetan Plateau. Their modelling results show that models with no upper décollement and/or with a strong frictional upper décollement deform in the in-sequence forward-breaking style. However, models with a strong basal décollement and weak upper décollement deform in the out-of-sequence style. Hence, the spatial relation of a strong basal and weak upper décollements may be one of the important factors producing the structural style.

Furthermore, there are several numerical models that have been applied to explain the tectonic evolution of thin-skinned fold-and-thrust belts. Morgan [2015] and Hughes [2020] highlighted the essential role of cohesive strength and residual strength of the basal décollement in the nucleation of discrete faults, the specific styles of structures that develop in fold-and-thrust belts using a series of 2D discrete element models. Also, Meng and Hodgetts [2019a,b] used 2D discrete element method to simulate thin-skinned tectonic deformation in stratigraphic sequences with two décollements, to yield new insights into the combined control of rock competence, depth and thickness of the upper décollement on structural styles and decoupling characteristics. In this regard, rock rheology and décollement layer thickness can greatly influence thin-skinned tectonics in systems with multiple décollements, and determine the degree of structural decoupling. Their DE-modelling results indicate models with a lower

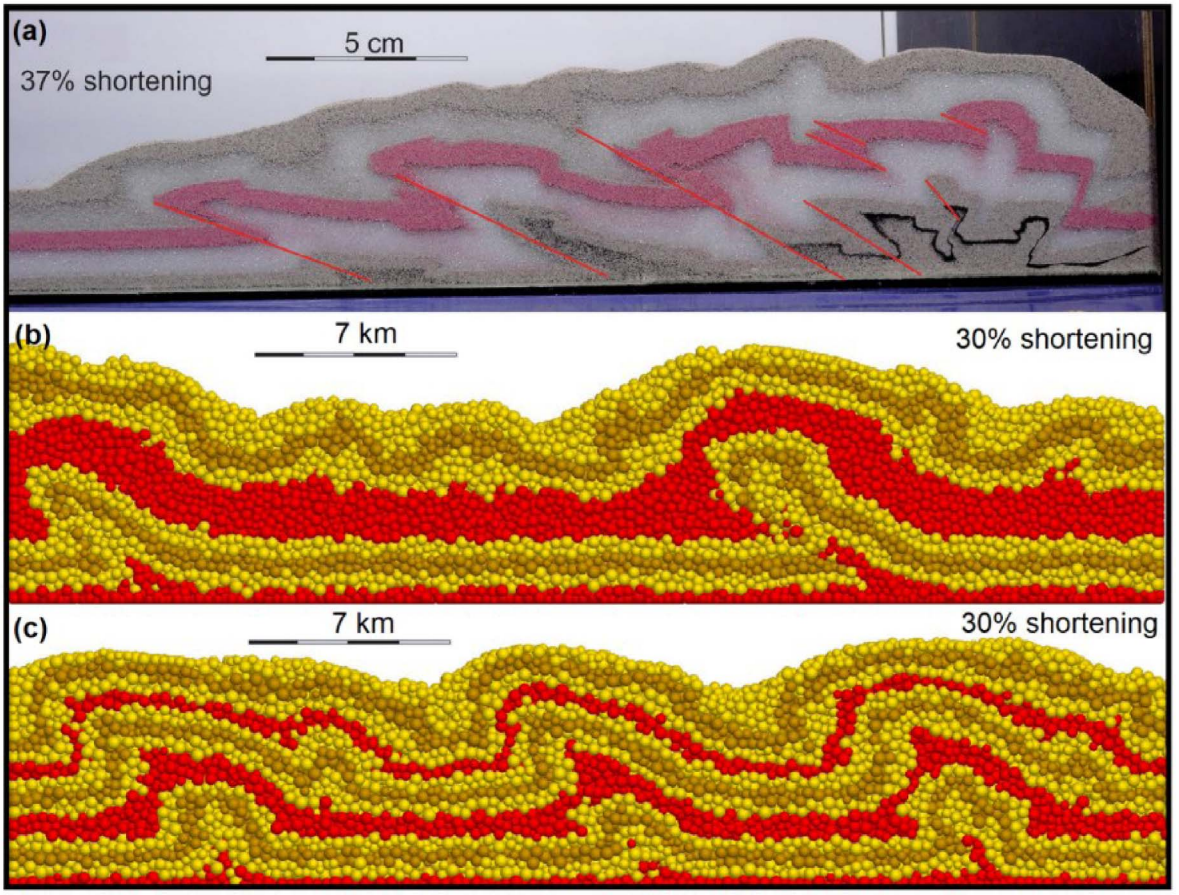


**Figure 9.** (a) Model 4 from the study conducted Ghanadian et al. [2017a,b] is compared to our modelling outcome (b) and (c). that are series 1 model 3d and series 6 model 2d from our numerical investigation respectively.

cohesion and a thinner décollement resulted in more distributed strain and a larger number of folds, whilst models with a higher cohesion and a thicker décollement led to localized shear zones in fewer folds. In addition, surface uplift and fold amplitude are mainly positively affected by the décollement thickness, so that, the greater the surface uplift and fold amplitude are developed in models with the thicker décollement [Meng and Hodgetts, 2019a,b] (such as Figure 10). We numerically obtained comparable results and similar evolution in model series 1 to 3 of the present study with basal and upper décollements within the cover sequence, which are structurally comparable with DE-models by Meng and Hodgetts [2019a,b]. Modelling results of the present study indicate that competent layers are characterized by localized strain zones as fault-bend, fault-propagation folds and pop-up structures with tensile fractures developed in fold hinges. Moreover, thicker intermediate and upper décollements can provide the higher the degree of decoupling, sufficient mobile materials to fill fold cores and development of disharmonic folds.

## 6. Conclusions

Thin-skinned fold–thrust belts commonly contain multiple décollements that exhibit first-order control on their evolution and structural styles. Décollements cause the fold style and fold–fault interactions to become more complex, as well as structures formed under the influence of décollements are the

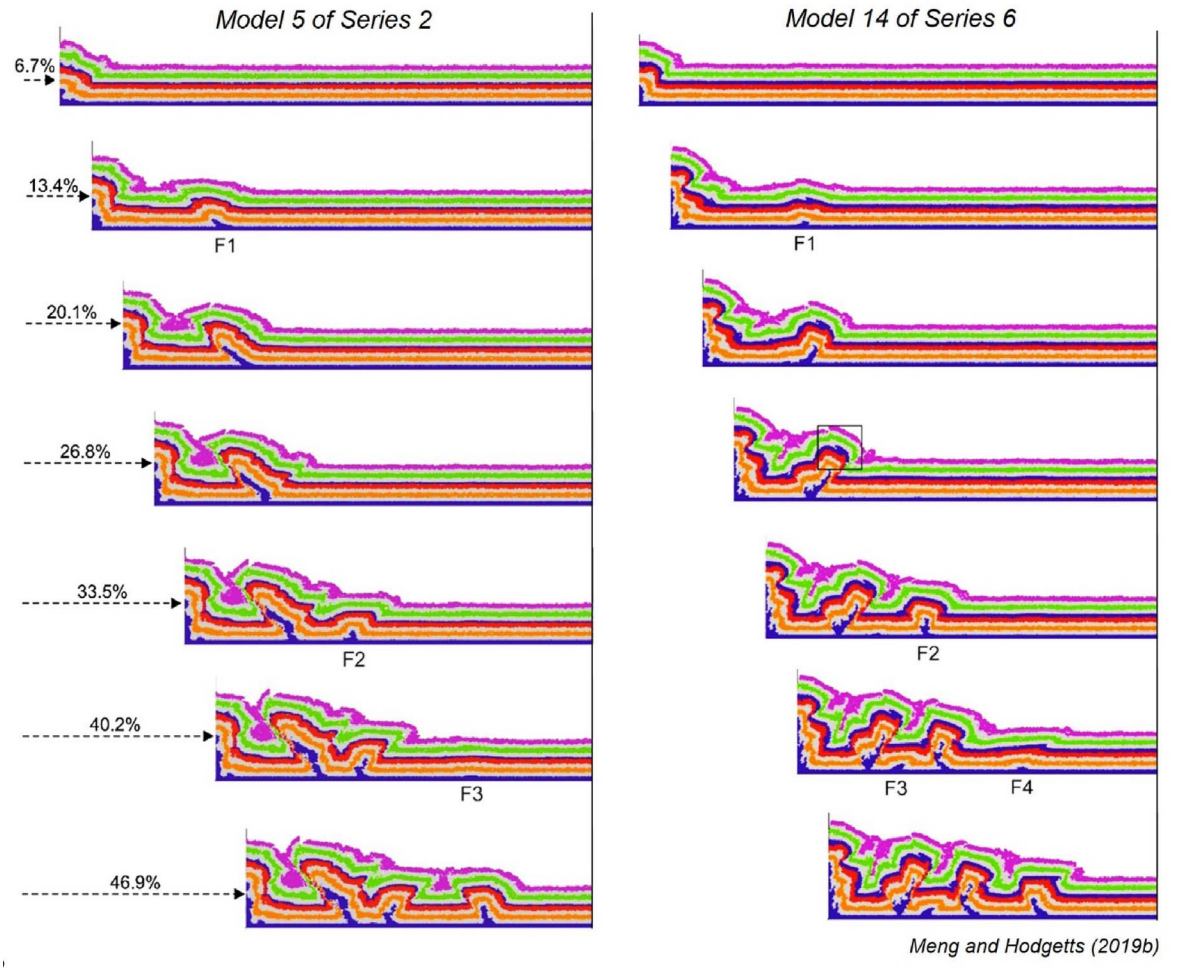


**Figure 10.** DE-modelling results of model 5 in series 2 with a thin upper décollement; and model 14 in series 6 with a thick upper décollement [after Meng and Hodgetts, 2019b].

locations where hydrocarbons can be found. Another known factor is the importance of mechanical property contrast between layers based on strength differences. As a result, numerical modelling is used as one of the methods available to better investigate the effect of the above variables. Therefore, in this paper, we focused on the role of a few core factors to study of the structural evolution of thin-skinned fold-and-thrust belts. We have used the discrete element method (DEM) to carry out a series of numerical models to analyze the differences in the structural evolution and style of thin-skinned fold-and-thrust belts causing from the thickness of décollements, the number of décollements, the rheological contrast. Finally, we tried to compare the resulting models to structures and kinematic features of natural structures, however we do not claim that these models exactly reflect natural structures.

As a result of horizontal shortening, a variety of fold styles, such as décollement, fold-bend and fold-propagation folds were generated by varying décollement thickness and cover rock cohesiveness. Thicker décollements can develop greater surface uplifts and provide sufficient materials to fill fold cores and development of disharmonic and larger folds in geometry. The presence of a thick intermediate décollement facilitated decoupling on cover rock, forming a significant contrast in the deformation pattern between

the underlying and overlying layers. The modelling result suggests that the presence of décollements and their number and mechanical properties are considered to be a key parameter in the evolution, structural style, deformation pattern and strain partitioning of thin-skinned fold-and-thrust belts. The modelling results are compatible with the Zagros fold-and-thrust belt, SW Iran, especially the Dezful Embayment zone, as well as previous analogue and numerical models, regarding the structural styles, indicating that the combination of increasing thickness in intermediate and upper décollements and a less-competent cover rock could preferentially produce a range of fold styles including sinusoidal, box, fault-propagation and fault-bend folds. This study demonstrates a strong influence of décollement thickness and rock mechanical properties on the structural styles of fold-and-thrust belts.

## Conflicts of interest

Authors have no conflict of interest to declare.

## Author contributions

NE: Project administration, Field work, Conceptualization, Methodology, Software, Formal analysis, Validation, Investigation, Visualization, Resources, Data Curation, Writing—original draft, review and editing. SAA: Supervision, Investigation, Resources, Data Curation. STN: Conceptualization, Conceptualization, Investigation, Visualization, Resources, Data Curation, Writing—review and editing. MRG: Resources, Writing—review and editing.

## Acknowledgements

The first author greatly thanks Professor Martin Schöpfer (University of Wien, Austria) for the excellent guidelines and feedback on an early version of modelling procedures.

## References

Alavi, M. (2004). Regional stratigraphy of the Zagros fold-thrust belt of Iran and its proforeland evolution. *Am. J. Sci.*, 304, 1–20.

Alavi, M. (2007). Structures of the Zagros fold-thrust belt in Iran. *Am. J. Sci.*, 307, 1064–1095.

Barcos, L., Díaz-Azpiroz, M., Balanyá, J. C., Expósito, I., Jiménez-Bonilla, A., and Faccenna, C. (2016). Analogue modelling of inclined, brittle-ductile transpression: Testing analytical models through natural shear zones (external Betics). *Tectonophysics*, 682, 169–185.

Benesh, N. P., Plesch, A., Shaw, J. H., and Frost, E. K. (2007). Investigation of growth fault bend folding using discrete element modeling: implications for signatures of active folding above blind thrust faults. *J. Geophys. Res. Solid Earth*, 112, article no. B03S04.

Borderie, S., Graveleau, F., Witt, C., and Vendeville, B. C. (2018). Impact of an interbedded viscous décollement on the structural and kinematic coupling in fold-and-thrust belts: Insights from analogue modeling. *Tectonophysics*, 722, 118–137.

Botter, C., Cardozo, N., Hardy, S., Lecomte, I., and Escalona, A. (2014). From mechanical modeling to seismic imaging of faults: A synthetic workflow to study the impact of faults on seismic. *Mar. Pet. Geol.*, 57, 187–207.

Buiter, S. J. (2012). A review of brittle compressional wedge models. *Tectonophysics*, 530, 1–17.

Burberry, C., Cosgrove, J., and Guo Liu, J. (2010). A study of fold characteristics and deformation style using the evolution of the land surface: Zagros Simply Folded Belt, Iran. In *Tectonic and Stratigraphic Evolution of Zagros and Makran during the Mesozoic–Cenozoic*, volume 330 of *Geological Society, London, Special Publications*. Geological Society of London.

Burbidge, D. R. and Braun, J. (2002). Numerical models of the evolution of accretionary wedges and fold-and-thrust belts using the distinct-element method. *Geophys. J. Int.*, 148(3), 542–561.

Caër, T., Souloumiac, P., Maillot, B., Leturmy, P., and Nussbaum, C. (2018). Propagation of a fold-and-thrust belt over a basement graben. *J. Struct. Geol.*, 115, 121–131.

Casas, A. M., Gapais, D., Naplas, T., Besnard, K., and Román-Berdiel, T. (2001). Analogue models of transpressive systems. *J. Struct. Geol.*, 23, 733–743.

Casciello, E., Vergés, J., Saura, E., Casini, G., Fernández, N., Blanc, E., Homke, S., and Hunt, D. W. (2009). Fold pattern and multilayer rheology of the Lurestan Province, Zagros Simply Folded Belt (Iran). *J. Geol. Soc.*, 166, 947–959.

Costa, E. and Vendeville, B. C. (2002). Experimental insights on the geometry and kinematics of fold-and-thrust belts above weak, viscous evaporitic décollement. *J. Struct. Geol.*, 24, 1729–1739.

Cotton, J. T. and Koyi, H. A. (2000). Modeling of thrust fronts above ductile and frictional detachments: Application to structures in the Salt Range and Potwar Plateau, Pakistan. *Geol. Soc. Am. Bull.*, 112, 351–363.

Cruz, L., Malinski, J., Wilson, A., Take, W. A., and Hilley, G. (2010). Erosional control of the kinematics and geometry of fold-and-thrust belts imaged in a physical and numerical sandbox. *J. Geophys. Res. Solid Earth*, 115, article no. B09404.

Cruz, L., Serrano, A. V., Fitz-Díaz, E., and Hudleston, P. (2019). Quantifying frictional variations and erosion in the Mexican fold-thrust belt. *J. Struct. Geol.*, 120, 1–13.

Cruz, L., Teyssier, C., Perg, L., Take, A., and Fayon, A. (2008). Deformation, exhumation, and topography of experimental doubly-vergent orogenic wedges subjected to asymmetric erosion. *J. Struct. Geol.*, 30, 98–115.

Cui, J., Jia, D., Yin, H., Chen, Z., Li, Y., Wang, M., Xiaogen, F., Shen, L., Sun, C., Ma, D., and Zhang, Y. (2019). The influence of a weak upper ductile detachment on the Longmen Shan fold-and-thrust belt (eastern margin of the Tibetan Plateau): Insights from sandbox experiments. *J. Asian Earth Sci.*, 198, article no. 104220.

Cui, J., Jia, D., Yin, H., Chen, Z., Li, Y., Wang, M., Xiaogen, F., Shen, L., Sun, C., Ma, D., and Zhang, Y. (2020). Corrigendum to "The influence of a weak upper ductile detachment on the Longmen Shan fold-and-thrust belt (eastern margin of the Tibetan Plateau): Insights from sandbox experiments". *J. Asian Earth Sci.*, 200, article no. 104507.

Cundall, P. A. and Strack, O. D. L. (1979). A discrete numerical model for granular assemblies. *Geotechnique*, 29(1), 47–65.

Dahlen, F. A. (1984). Noncohesive critical Coulomb wedges: an exact solution. *J. Geophys. Res. Solid Earth*, 89, article no. 10125.

Dahlen, F. A. (2003). Critical taper model of fold-and-thrust belts and accretionary wedges. *Annu. Rev. Earth Planet. Sci.*, 18, 55–99.

Dal Zilio, L., Ruh, J., and Avouac, J.-P. (2020). Structural evolution of orogenic wedges: Interplay between erosion and weak décollements. *Tectonics*, 39, article no. e2020TC006210.

Davis, D., Suppe, J., and Dahlen, F. A. (1983). Mechanics of fold-and-thrust belts and accretionary wedges. *J. Geophys. Res. Atmos.*, 88, 1153–1172.

Davis, D. M. and Engelder, T. (1985). The role of salt in fold-and-thrust belts. *Tectonophysics*, 119, 67–88.

Del Ventisette, C., Bonini, M., Maestrelli, D., Sani, F., Lavarone, E., and Montanari, D. (2021). 3D-thrust fault pattern control on negative inversion: An analogue modelling perspective on central Italy. *J. Struct. Geol.*, 143, article no. 104254. ISSN 0191-8141.

Derikvand, B., Alavi, S. A., Abdollahie Fard, I., and Hajialibeigi, H. (2018). Folding style of the Dezful Embayment of Zagros Belt: Signature of detachment horizons, deep-rooted faulting and syndeformation deposition. *Mar. Pet. Geol.*, 91, 501–518.

Derikvand, B., Alavi, S. A., Fard, I. A., and Jalali, L. (2019). Changing in fold geometry from faulted detachment fold to fault-bend fold, a case study: The Zeloi Anticline in the Dezful Embayment, southwest of Iran. *J. Pet. Sci. Eng.*, 173, 381–401.

Driehaus, L., Naplas, T., and Ballard, J. F. (2014). Interaction between deformation and sedimentation in a multidecollement thrust zone: analogue modelling and application to the Sub-Andean thrust belt of Bolivia. *J. Struct. Geol.*, 65, 59–68.

Eslamirezaei, N., Alavi, S. A., Nabavi, S. T., and Ghassemi, M. R. (2022). Understanding the role of décollement thickness on the evolution of décollement folds: insights from discrete element models. *C. R. Géosci.*, 354, 75–91.

Farzipour-Saein, A. (2017). Folding style controlled by intermediate decollement thickness change in the Lurestan region (NW of the Zagros fold-and thrust belt), using analogue models. *Int. J. Earth Sci.*, 106, 1525–1537.

Farzipour-Saein, A. and Koyi, H. (2014). Effect of lateral thickness variation of an intermediate decollement on the propagation of deformation front in the Lurestan and Izeh zones of the Zagros fold-thrust belt, insights from analogue modeling. *J. Struct. Geol.*, 65, 17–32.

Fossen, H. (2016). *Structural Geology*. Cambridge University Press, Cambridge, 2nd edition.

Ghanadian, M., Faghih, A., Fard, I. A., Kusky, T., and Maleki, M. (2017a). On the role of incompetent strata in the structural evolution of the Zagros

FoldThrust Belt, Dezful Embayment, Iran. *Mar. Pet. Geol.*, 81, 320–333.

Ghanadian, M., Faghih, A., Grasemann, B., Fard, I. A., and Maleki, M. (2017b). Analogue modeling of the role of multi-level decollement layers on the geometry of orogenic wedge: an application to the Zagros Fold—Thrust Belt, SW Iran. *Int. J. Earth Sci.*, 106, 2837–2853.

Ghosh, S., Bose, S., Mandal, N., and Laik, A. (2020). Mid-crustal ramping of the Main Himalayan Thrust in Nepal to Bhutan Himalaya: New insights from analogue and numerical experiments. *Tectonophysics*, 782–783, article no. 228425. ISSN 0040-1951.

Graveleau, F., Malavieille, J., and Dominguez, S. (2012). Experimental modelling of orogenic wedges: A review. *Tectonophysics*, 538–540, 1–66.

Gu, Z., Wang, X., Nunns, A., Zhang, B., Jiang, H., Fu, L., and Zhai, X. (2021). Structural styles and evolution of a thin-skinned fold-and-thrust belt with multiple detachments in the eastern Sichuan Basin, South China. *J. Struct. Geol.*, 142, article no. 104191.

Hardy, S. (2019). Discrete element modelling of extensional, growth, fault-propagation folds. *Basin Res.*, 31, 584–599.

Hardy, S. and Finch, E. (2005). Discrete-element modelling of detachment folding. *Basin Res.*, 17, 507–520.

Hardy, S. and Finch, E. (2006). Discrete element modelling of the influence of cover strength on basement-involved fault-propagation folding. *Tectonophysics*, 415, 225–238.

Hardy, S., McClay, K., and Munoz, J. A. (2009). Deformation and fault activity in space and time in high-resolution numerical models of doubly vergent thrust wedges. *Mar. Pet. Geol.*, 26, 232–248.

Heydarzadeh, K., Hajialibeigi, H., Vergés, J., and Gharabeigli, G. (2021). Tectono-sedimentary evolution of the Dehdasht structural basin (Central Zagros, Iran). *Tectonophysics*, 806, article no. 228791.

Heydarzadeh, K., Ruh, J. B., Vergés, J., Hajialibeigi, H., and Gharabeigli, G. (2020). Evolution of a structural basin: Numerical modelling applied to the Dehdasht Basin, Central Zagros, Iran. *J. Asian Earth Sci.*, 187, article no. 104088. ISSN 1367-9120.

Homza, T. X. and Wallace, W. K. (1995). Geometric and kinematic models for detachment folds with fixed and variable detachment depths. *J. Struct. Geol.*, 17, 575–588. ISSN 0191-8141.

Hughes, A. N. (2020). Mechanical controls on structural styles in shortening environments: A discrete-element modelling approach. In Hammerstein, J. A., Di Cuia, R., Cottam, M. A., Zamora, G., and Butler, R. W. H., editors, *Fold and Thrust Belts; Structural Styles, Evolution and Exploration*, volume 490 of *Geological Society of London Special Publications*, pages 33–55. Geological Society of London.

Hughes, A. N., Benesh, N. P., and Shaw, J. H. (2014). Factors that control the development of fault-bend versus fault-propagation folds: insights from mechanical models based on the discrete element method (DEM). *J. Struct. Geol.*, 68, 121–141.

Hughes, A. N. and Shaw, J. H. (2015). Insights into the mechanics of fault-propagation folding styles. *Geol. Soc. Am. Bull.*, 127(11–12), 1752–1765.

Humair, F., Bauville, A., Epard, J. L., and Schmalholz, S. (2020). Interaction of folding and thrusting during fold-and-thrust-belt evolution: Insights from numerical simulations and application to the Swiss Jura and the Canadian Foothills. *Tectonophysics*, 789, article no. 228474. ISSN 0040-1951.

Ito, G. and Moore, G. F. (2021). Widths of imbricate thrust blocks and the strength of the front of accretionary wedges and fold-and-thrust belts. *Tectonophysics*, 799, article no. 228704.

Konstantinovskaya, E. and Malavieille, J. (2011). Thrust wedges with décollement levels and syntectonic erosion: A view from analog models. *Tectonophysics*, 502, 336–350.

Koyi, H. and Sans, M. R. (2003). Modelling the effect of multiple detachments in fold-thrust belts. In *AAPG International Meeting*.

Koyi, H. A., Hessami, K., and Teixell, A. (2000). Epicenter distribution and magnitude of earthquakes in fold-thrust belts: insights from sandbox models. *Geophys. Res. Lett.*, 27(2), 273–276.

Koyi, H. A. and Maillot, B. (2007). Tectonic thickening of hanging-wall units over a ramp. *J. Struct. Geol.*, 29, 924–932.

Koyi, H. A. and Mansurbeg, H. (2021). The role of multiple weak lithologies in the deformation of cover units in the northwestern segment of the Zagros fold-and-thrust belt. *J. Petrol. Geol.*, 44, 145–166.

Lacombe, O., Ruh, J., Brown, D., and Nilfouroushan, F. (2016). Introduction: Tectonic evolution and

mechanics of basement-involved fold-and-thrust belts. *Geol. Mag.*, 153, 759–762.

Leever, K. A., Gabrielsen, R. H., Sokoutis, D., and Willingshofer, E. (2011). The effect of convergence angle on the kinematic evolution of strain partitioning in transpressional brittle wedges: Insights from analog modeling and high-resolution digital image analysis. *Tectonics*, 30, article no. TC2013.

Li, J. and Mitra, S. (2017). Geometry and evolution of fold-thrust structures at the boundaries between frictional and ductile detachments. *Mar. Pet. Geol.*, 85, 16–34.

Maillot, B. and Koyi, H. A. (2006). Thrust dips and thrust refraction in fault-bend faults: analogue experiments and theoretical predictions. *J. Struct. Geol.*, 28, 36–49.

McClay, K. R., Whitehouse, P. S., Dooley, T., and Richards, M. (2004). 3D evolution of fold and thrust belts formed by oblique convergence. *Mar. Pet. Geol.*, 21, 857–877.

Meng, Q. and Hodgetts, D. (2019a). Structural styles and decoupling in stratigraphic sequences with double décollements during thin-skinned contractional tectonics: Insights from numerical modelling. *J. Struct. Geol.*, 127, article no. 103862. ISSN 0191 8141.

Meng, Q. and Hodgetts, D. (2019b). Combined control of décollement layer thickness and cover rock cohesion on structural styles and evolution of fold belts: A discrete element modelling study. *Tectonophysics*, 757, 58–67.

Mitra, S. (2003). A unified kinematic model for the evolution of detachment folds. *J. Struct. Geol.*, 25, 1659–1673.

Mohammadrezaei, H., Alavi, S. A., Ghanadian, M., and Ghassemi, M. R. (2022). The effects of wrench-dominated basement-involved faults on folding of overlying strata in the Bahregansar anticline, western Persian Gulf, Iran. *C. R. Géosci.*, 354, 105–118.

Morgan, J. K. (2015). Effects of cohesion on the structural and mechanical evolution of fold and thrust belts and contractional wedges: Discrete element simulations. *J. Geophys. Res. Solid Earth*, 120, 3870–3896.

Mouthereau, F., Lacombe, O., and Meyer, B. (2006). The Zagros folded belt (Fars, Iran): constraints from topography and critical wedge modelling. *Geophys. J. Int.*, 165, 336–356.

Mouthereau, F., Lacombe, O., and Vergés, J. (2012). Building the Zagros collisional orogen: timing, strain distribution and the dynamics of Arabia/Eurasia plate convergence. *Tectonophysics*, 532, 27–60.

Nabavi, S. T., Alavi, S. A., Díaz-Azpiroz, M., Mohammadi, S., Ghassemi, M. R., Fernández, C., Barcos, L., and Frehner, M. (2020). Deformation mechanics in inclined, brittle-ductile transpression zones: insights from 3D finite element modelling. *J. Struct. Geol.*, 137, article no. 104082.

Nabavi, S. T., Alavi, S. A., Mohammadi, S., and Ghassemi, M. R. (2018). Mechanical evolution of transpression zones affected by fault interactions: insights from 3D elasto-plastic finite element models. *J. Struct. Geol.*, 106, 19–40.

Nabavi, S. T., Díaz-Azpiroz, M., and Talbot, C. J. (2017a). Inclined transpression in the Neka Valley, eastern Alborz, Iran. *Int. J. Earth Sci.*, 106, 1815–1840.

Nabavi, S. T. and Fossen, H. (2021). Fold geometry and folding – a review. *Earth Sci. Rev.*, 222, article no. 103812. ISSN 0012-8252.

Nabavi, S. T., Rahimi-Chakdel, A., and Khademi, M. (2017b). Structural pattern and emplacement mechanism of the Neka Valley nappe complex, eastern Alborz, Iran. *Int. J. Earth Sci.*, 106, 2387–2405.

Najafi, M., Beamud, E., Ruh, J., Mouthereau, F., Tahmasbi, A., Bernaola, G., Yassaghi, A., Motamedi, H., Sherkati, S., Goodarzi, M. G. H., and Vergés, J. (2021). Pliocene growth of the Dowlatabad syncline in Frontal Fars arc: Folding propagation across the Zagros Fold Belt, Iran. *Geol. Soc. Am. Bull.*, 133, 1381–1403.

Nilforoushan, F., Pysklywec, R., and Cruden, A. (2012). Sensitivity analysis of numerical scaled models of fold-and-thrust belts to granular material cohesion variation and comparison with analog experiments. *Tectonophysics*, 526–529, 196–206.

Nilforoushan, F., Pysklywec, R., Cruden, A., and Koyi, H. (2013). Thermal-mechanical modeling of salt-based mountain belts with pre-existing faults: Applications to the Zagros fold and thrust belt, southwest Iran. *Tectonics*, 32, 1212–1226.

Pichot, T. and Nalpas, T. (2009). Influence of synkinematic sedimentation in a thrust system with two decollement levels; analogue modelling. *Tectonophysics*, 473, 466–475.

Pla, O., Roca, E., Xie, H., Izquierdo-Llavall, E., Muñoz, J. A., Rowan, M. G., Ferrer, O., Gratacós, Ò., Yuan, N., and Huang, S. (2019). Influence of syntectonic sedimentation and décollement rheology on the geometry and evolution of orogenic wedges: analogue modeling of the Kupa fold-and-thrust belt (NW China). *Tectonics*, 38, 2727–2755.

Rosas, F. M., Duarte, J. C., Almeida, P., Schellart, W. P., Riel, N., and Terrinha, P. (2017). Analogue modelling of thrust systems: Passive vs. active hanging wall strain accommodation and sharp vs. smooth fault-ramp geometries. *J. Struct. Geol.*, 99, 45–69.

Ruh, J. B., Gerya, T., and Burg, J. P. (2013). High-resolution 3D numerical modeling of thrust wedges: Influence of décollement strength on transfer zones. *Geochem. Geophys. Geosyst.*, 14, 1131–1155.

Ruh, J. B., Gerya, T., and Burg, J.-P. (2014). 3D effects of strain vs. velocity weakening on deformation pattern in accretionary wedges. *Tectonophysics*, 615–616, 122–141.

Ruh, J. B., Gerya, T., and Burg, J.-P. (2017). Toward 4D modeling of orogenic belts: Example from the transpressive Zagros Fold Belt. *Tectonophysics*, 702, 82–89.

Ruh, J. B., Kaus, B. J., and Burg, J.-P. (2012). Numerical investigation of deformation mechanics in fold-and-thrust belts: Influence of rheology of single and multiple décollements. *Tectonics*, 31, article no. TC3005.

Schori, M., Mosar, J., and Schreurs, G. (2015). Multiple detachments during thin-skinned deformation of the Swiss Central Jura: a kinematic model across the Chasseral. *Swiss J. Geosci.*, 108, 327–343.

Sepehr, M. and Cosgrove, J. W. (2004). Structural framework of the Zagros Fold–Thrust Belt, Iran. *Mar. Petrol. Geol.*, 21, 829–843.

Shamszadeh, A., Sarkarinejad, K., Ferrer, O., Mukherjee, S., and Seraj, M. (2022a). Effect of inherited structural highs on the structure and kinematics of the South Dezful Embayment, SW Iran. *Geol. Mag.*, 159, 1744–1766.

Shamszadeh, A., Sarkarinejad, K., Ferrer, O., Mukherjee, S., and Seraj, M. (2022b). Interaction of inherited structures and contractional deformation in the South Dezful Embayment: Insights from the Gachsaran oilfield, SW Iran. *Mar. Pet. Geol.*, 145, article no. 105871.

Sherkati, S., Letouzey, J., and Frizon de Lamotte, D. (2006). Central Zagros fold-thrust belt (Iran): new insights from seismic data, field observation and sandbox modeling. *Tectonics*, 25, article no. TC4007.

Sherkati, S., Molinaroc, M., Lamottec, D. F., and Letouzeyb, J. (2005). Detachment folding in the Central and Eastern Zagros fold-belt (Iran): salt mobility, multiple detachments and late basement control. *J. Struct. Geol.*, 27, 1680–1696.

Smart, K. J., Wyrick, D. Y., and Ferrill, D. A. (2011). Discrete element modeling of Martian pit crater formation in response to extensional fracturing and dilational normal faulting. *J. Geophys. Res. Planets*, 116, article no. E04005.

Smit, J. H. W., Brun, J. P., and Sokoutis, D. (2003). Deformation of brittle-ductile thrust wedges in experiments and nature. *J. Geophys. Res. Solid Earth*, 108, 1–18.

Stockmal, G. S., Beaumont, C., Nguyen, M., and Lee, B. (2007). Mechanics of thin-skinned fold-and-thrust belts: Insights from numerical models. In Sears, J. W., Harms, T. A., and Evenchick, C. A., editors, *Whence the Mountains? Inquiries into the Evolution of Orogenic Systems: A Volume in Honor of Raymond A. Price*, volume 433 of *Geological Society of America Special Paper*, pages 63–98. Geological Society of America.

Sun, C., Li, Z., Wu, S., He, Z., Zhao, S., and Wang, P. (2021). Structural significance of the mid-level Décollement within the Western Sichuan Fold-And-Thrust Belt (WSFTB), insights from sandbox modeling. *Front. Earth Sci.*, 9, article no. 631405.

Vergés, J., Goodarzi, M. G. H., Emami, H., Karpuz, R., Efstathiou, J., and Gillespie, P. (2011). Multiple detachment folding in Pusht-e Kuh arc, Zagros: role of mechanical stratigraphy. In McClay, K., Shaw, J., and Suppe, J., editors, *Thrust Fault Related Folding*, volume 94 of *AAPG Memoir*, pages 69–94. American Association of Petroleum Geologists.

Verlet, L. (1967). Computer "Experiments" on classical fluids. I. Thermodynamical properties of Lennard-Jones molecules. *Phys. Rev.*, 159(1), 98–103. Bibcode:1967PhRv.159...98V.

Watkins, H., Bond, C. E., and Butler, R. W. H. (2014). Identifying multiple detachment horizons and an evolving thrust history through cross-section restoration and appraisal in the Moine Thrust Belt, NW Scotland. *J. Struct. Geol.*, 66, 1–10.

Wilkerson, M. S., Smaltz, S. M., Bowman, D. R., Fischer, M. P., and Higuera-Diaz, I. C. (2007). 2-D and 3-D modeling of detachment folds with hinterland inflation: A natural example from the Monterrey Salient, northeastern Mexico. *J. Struct. Geol.*, 29, 73–85.

Wu, J. E. and McClay, K. R. (2011). Two-dimensional analog modeling of fold and thrust belts: Dynamic interactions with syncontractional sedimentation and erosion. In McClay, K. R., Shaw, J., and Suppe, J., editors, *Thrust Fault-Related Folding*, volume 94 of *AAPG Memoir*, pages 301–333. American Association of Petroleum Geologists.

Xu, W., Yin, H., Jia, D., Li, C., Wang, W., Yang, G., He, W., Chen, Z., and Ren, R. (2021). Structural features and evolution of the northwestern Sichuan Basin: Insights from discrete numerical simulations. *Front. Earth Sci.*, 9, article no. 653395.

Yosefnejad, D. M., Nagel, T. J., and Froitzheim, N. (2017). Three-dimensional modelling of folds, thrusts, and strike-slip faults in the area of Val de Ruz (Jura Mountains, Switzerland). *Swiss J. Geosci.*, 110, 613–630.